Phase sensitive detection of vibrational optical activity free-induction-decay: vibrational CD and ORD

Hanju Rhee,[1,2] Young-Gun June,[1] Zee Hwan Kim,[1] Seung-Joon Jeon,[1,3] and Minhaeng Cho[1,2,3,*]

[1]*Department of Chemistry, Korea University, Seoul 136-701, South Korea*
[2]*Center for Multidimensional Spectroscopy, Korea University, Seoul 136-701, South Korea*
[3]*Multidimensional Spectroscopy Laboratory, Korea Basic Science Institute, Seoul 136-713, South Korea*
[*]*Corresponding author: mcho@korea.ac.kr*

Received January 23, 2009; revised March 9, 2009; accepted March 10, 2009;
posted March 12, 2009 (Doc. ID 106661); published April 16, 2009

Optical activity is manifested by chiral molecules including natural products and drugs, so that circular dichroism (CD) and optical rotatory dispersion (ORD) measurements can provide invaluable information on their chiro-optical properties and structures. It is experimentally demonstrated that heterodyne-detected Fourier-transform spectral interferometry with a femtosecond infrared pulse can be used to fully characterize the phase and amplitude of vibrational optical activity free-induction-decay field. The measured spectral interferograms are then converted to the linear optical activity susceptibility whose imaginary and real parts correspond to vibrational CD and ORD spectra. Unlike the conventional differential measurement technique, the present method based on a heterodyned interferometry is shown to be quite robust and stable. We anticipate that the present vibrational optical activity measurement technique will be of critical use in elucidating chiro-optical properties and structural changes in biomolecules. © 2009 Optical Society of America

OCIS codes: 300.6340, 300.6530.

1. INTRODUCTION

Circular dichroism (CD) and optical rotatory dispersion (ORD) are distinct chiro-optical properties manifested by almost all biomolecules, pharmaceutical drugs, and so on. Although they are related to each other via the Kramers-Kronig transformation [1], the relevant physical observables are measured in different ways. CD is the differential absorption of left- and right-circularly polarized (LCP and RCP) lights, whereas ORD is related to the measurement of the optical rotation angle of a linearly polarized beam. Recently, we have demonstrated that femtosecond characterization of vibrational optical activity (CD and ORD) could be accomplished by detecting coherently emitted optical activity (OA) free-induction-decay (FID) (OA-FID) field with a cross-polarization detection scheme [2,3]. Heterodyne-detected Fourier-transform (FT) spectral interferometry (FTSI) [4–12] was used to completely characterize the spectral phase and amplitude of OAFID with respect to a reference field. From the measured complex OAFID fields, it was possible to determine the linear OA susceptibility, $\Delta\chi(\omega)$ $[\equiv\chi_L(\omega)-\chi_R(\omega)]$, of which imaginary and real parts correspond to the CD and ORD spectra, respectively. Moreover, by detecting much weaker vibrational OA (VOA) signal than the electronic one, we successfully demonstrated that our femtosecond VOAFID measurement method [3] is quite useful and would be applicable to ultrafast time-resolved vibrational CD (VCD) studies.

The FTSI method has been proven to be useful for determining the phase and amplitude of unknown electric field [4,5] and recently used to characterize a variety of linear [4–7] and nonlinear [8–13] optical signal fields. Particularly, it is far more sensitive than any other well-known characterization techniques such as FROG [14], SPIDER [15], and so on, because it does not involve nonlinear optical processes. The heterodyned FTSI of OAFID has several advantages in comparison to conventional CD measurement methods utilizing polarization-modulation technique. First, the former is quite robust to incident beam (laser pulse) intensity fluctuation because it does not rely on a differential measurement scheme. Second, the optical heterodyning with a strong reference field enables to coherently amplify the weak OA signal with excellent signal-to-noise ratio, which allows one to shorten the data collection time. Third, the ORD spectrum in addition to the CD is simultaneously obtained without additional and independent measurement of frequency-dependent optical rotation angle or Kramers-Kronig transformation of the CD spectrum. Lastly, the method intrinsically has ultrafast time-resolving capability because the OA information is obtained from the time-domain OAFID field created by a femtosecond pulse. Note that the technique does not need polarization modulation of pulses, so that a sensitive pump pulse modulation technique can be used to boost the detection limit in time-resolved CD measurements.

Despite these advantages, a few technical problems should be resolved in the future. One of the main obstacles is that extremely small extinction ratio of polarizers is required to remove a large achiral contribution. For example, with ΔA (VCD)$=10^{-4}-10^{-5}$ at A (absorbance) ~ 1, polarizers with extinction ratio (ρ) better than $\sim 10^{-9}$

are needed, but such polarizers with sufficiently wide spectral ranges are not easily available. Note that our initial proof-of-principle experiment [3] relied on a special dichroic absorptive polarizer (calcite plate) with fairly restricted spectral windows (3.35–3.5 and 3.9–4.1 μm, etc.). Low-quality polarizer pair may introduce a large achiral background contribution that significantly contaminates the pure chiral signal. However, the phase of the CD component of the OAFID field differs from that of the achiral component after the output polarizer by 90°, so that it is possible to separate them using the phase sensitive FTSI method. This aspect will be discussed later in detail. In practice, since the heterodyne-detected FTSI based on a Mach-Zehnder interferometer is vulnerable to the fluctuation of optical path difference between two arms of the interferometer, its stability is a crucial factor for separating real and imaginary components of the FID field, which have different phases.

In this paper, we will first present a brief account of recent theoretical description of a cross-polarization detection scheme, which shows how the OA susceptibility is connected to the measured FID signal fields. Then, a few essential aspects of the heterodyned FTSI method, including the detection and characterization of the FID fields, will be discussed in detail, and VCD and vibrational ORD (VORD) experimental results of small chiral molecules, e.g., (R)-limonene and (1S)-β-pinene will be presented. To investigate the influences of laser intensity and phase fluctuations on the retrieved VCD signal, numerical simulations at both optically perfect and imperfect conditions were carried out. Finally, we will present experimental evidence that the phase sensitive detection of VCD signal is feasible even when the weak VOAFID signal is masked by much larger achiral background contribution originating from optical imperfection.

2. METHOD

The present VOAFID measurement is achieved by two stages: the VOAFID field generation from the cross-polarization setup and the subsequent heterodyned detection. In our theoretical work [2], it was shown that the parallel and perpendicular components $\tilde{E}^{\mathrm{FID}}_{\parallel,\perp}(\omega)$ of the emitted FID field are related to each other via the complex OA susceptibility as

$$\tilde{E}^{\mathrm{FID}}_{\perp}(\omega) = \frac{\pi\omega L}{cn(\omega)}\Delta\chi(\omega)\tilde{E}^{\mathrm{FID}}_{\parallel}(\omega), \tag{1}$$

where $n(\omega)$, c, and L are the index of refraction, the velocity of light in vacuum, and the sample length, respectively. The cross-polarization-detected electric field $\tilde{E}^{\mathrm{FID}}_{\perp}(\omega)$ is the chiral OAFID field, whereas the parallel one $\tilde{E}^{\mathrm{FID}}_{\parallel}(\omega)$ is the transmitted field produced by the interference between the achiral electric-dipole-allowed optical FID and the input pulse. Equation (1) indicates that, even though $\tilde{E}^{\mathrm{FID}}_{\perp}$ contains the entire chiral information, the additional achiral component $\tilde{E}^{\mathrm{FID}}_{\parallel}$ should be characterized to completely retrieve the CD [imaginary part of $\Delta\chi(\omega)$] and ORD [real part of $\Delta\chi(\omega)$] spectra. Both FID fields are then spectral-interferometrically heterodyne-detected with a preceding reference field.

The VOAFID measurement setup is depicted in Fig. 1. The femtosecond IR pulse (1 kHz 2 μJ 60 fs IR pulse with the center frequency of ~2900 cm^{-1}) used for the present experiment was generated by using the difference-frequency mixing of the signal and idler pulses of a femtosecond optical parametric amplifier (OPA-800C, Spectra Physics). This IR pulse train is separated by a wedged ZnSe window and injected to the signal and reference arms of the Mach-Zehnder interferometer [16]. In the signal arm, the IR pulse is used to create vibrational coherence in the sample and then the FID field is emitted from the chiral sample placed between two polarizers LP1 and LP2. The pulse in the reference arm serves as a strong reference field for a subsequent heterodyne detection. In Secs. 2.A–2.C, the essential elements and characteristics of this heterodyne-detected FTSI method will be presented and discussed in more detail.

A. Cross-Polarization Beam Configuration

To measure the typically weak VOA signal ($\Delta A = 10^{-4}-10^{-5}$ at $A \sim 1$) as purely as possible in the cross-polarization configuration shown in Fig. 1, it is critical to choose a pair of crossed polarizers (LP1 and LP2) with extinction ratio smaller than ~10^{-9}. It is known that calcite polarizer (dichroic absorption type) meets this criterion in limited IR ranges that cover C-H stretching vibration region [17]. Thus, we used 1 mm calcite plates (LP1 and LP2) as a pair of main polarizers. However, because the input pulse spectrum is broader than the effective working frequency range of the calcite polarizer (2840–2980 cm^{-1}), a significant amount of unfiltered light outside this spectral range leaks through the crossed calcite polarizer pair, which can largely contribute to the chiral VOAFID signal as a background noise. Note that the level of stray light in a standard monochromator is typically ~10^{-5} of the incident light intensity (I) and consequently it overpowers the weak VOAFID signal ($I_{\perp}$

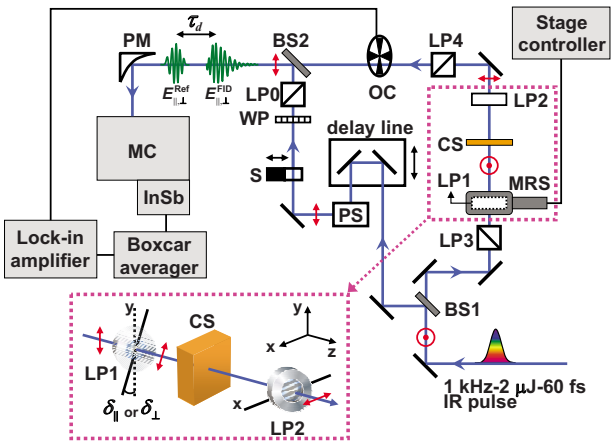

Fig. 1. (Color online) Experimental setup for the VOAFID measurement. BS1 (wedged ZnSe window) and BS2 (wedged CaF_2 window), beamsplitters; PS, periscope; LP0, LP3 and LP4, rutile prism polarizers; LP1 and LP2, calcite plate polarizers; MRS, motorized rotational stage (LP1 is attached to MRS); WP, wire-grid polarizer; CS, chiral sample; OC, optical chopper; S, shutter; PM, parabolic mirror; MC, monochromator; and InSb, indium antimonide single-element IR detector.

$\sim 10^{-9} I_{\parallel}$) inside the working spectral window. To eliminate such a large unwanted contribution, we used an additional pair of crossed rutile prism polarizers (LP3 and LP4). Their extinction ratio is $\sim 2\times 10^{-6}$ in the wavelength range from 2.5 to 4 μm, which covers the entire IR pulse spectrum, so that the substantial noise suppression by a factor of 2×10^{-11} (portion of stray light $\times$ extinction ratio of rutile polarizer) was achieved. Both polarizer pairs (calcite and rutile) have the same perpendicular geometries. That is to say, the transmission axes of LP1 and LP3 lie in the vertical direction, whereas those of the LP2 and LP4 are in the horizontal direction. To achieve optimal perpendicularity between LP1 and LP2 transmission axes, a high-resolution motorized rotational stage (MRS) (Newport) was used to finely control the orientation of LP1 with an incremental resolution of 0.0005°.

As can be seen in Eq. (1), the vertical electric field component $\tilde{E}_{\parallel}^{\mathrm{FID}}$ in addition to $\tilde{E}_{\perp}^{\mathrm{FID}}$ needs to be measured for the complete characterization of $\Delta\chi(\omega)$. To measure $\tilde{E}_{\parallel}^{\mathrm{FID}}$, LP2 should be rotated by 90° such that its transmission axis is parallel to the LP1 axis. Due to technical reasons and for the sake of experimental simplicity that will be discussed later, however, we instead rotated LP1 by a small angle $\delta_{\parallel}=0.5°$ from the cross-polarization configuration and this partial rotation allows only a small amount of $\tilde{E}_{\parallel}^{\mathrm{FID}}$ to be leaked through LP2 and LP4 (see Fig. 1 for the definition of $\delta_{\parallel}$ angle). Although the transmitted field in such a geometry contains both achiral $\tilde{E}_{\parallel}^{\mathrm{FID}}$ and chiral $\tilde{E}_{\perp}^{\mathrm{FID}}$, it mostly reflects the electric-dipole-allowed optical FID $\tilde{E}_{\parallel}^{\mathrm{FID}}$, because the partially transmitted $\tilde{E}_{\parallel}^{\mathrm{FID}}$ is about two orders of magnitude larger than $\tilde{E}_{\perp}^{\mathrm{FID}}$. Note that the magnitude ratio of the partial $\tilde{E}_{\parallel}^{\mathrm{FID}}$ to $\tilde{E}_{\perp}^{\mathrm{FID}}$ is estimated to be about 200:1 by the Malus law [18] when $\delta_{\parallel}=0.5°$. Thus, the opening of LP1 by $\delta_{\parallel}=0.5°$ is enough to measure the achiral FID field $\tilde{E}_{\parallel}^{\mathrm{FID}}$ when it is necessary.

B. Heterodyne-Detected FTSI

The other pulse reflected at the ZnSe window propagates in the second arm of the Mach-Zehnder interferometer and was used as reference field $\tilde{E}_{\perp}^{\mathrm{Ref}}(\omega)$ to amplify and interferometrically characterize both $\tilde{E}_{\perp}^{\mathrm{FID}}(\omega)$ and $\tilde{E}_{\parallel}^{\mathrm{FID}}(\omega)$. For the spectral interferometric detection, a delay line was used to properly adjust the optical path difference between the two arms, so that the reference pulse precedes $\tilde{E}_{\perp}^{\mathrm{FID}}(\omega)$ or $\tilde{E}_{\parallel}^{\mathrm{FID}}(\omega)$ by a time delay τ_d ($\sim$1 ps in the present case). The reference pulse passed through two polarizers [wire-grid polarizer (WP) and LP0] and then was combined with $\tilde{E}_{\perp}^{\mathrm{FID}}(\omega)$ or $\tilde{E}_{\parallel}^{\mathrm{FID}}(\omega)$ at a wedged CaF_2 window. Here, the WP serves as an attenuator of the reference pulse and the LP0 cleans up the polarization state of the reference pulse for an efficient heterodyne detection of the FID field.

The combined beam was focused by a parabolic mirror (PM) onto an entrance slit of a monochromator (TriaX 190, Horiba Jobin Yvon) and dispersed by a grating (120 grooves per mm, 5 μm blazed). The total spectral interferogram $S_{\parallel,\perp}(\omega)$ produced by the interference between the time-separated FID signal and reference fields was recorded by scanning the monochromator by 4 nm interval and by detecting the dispersed signal by an LN_2-cooled InSb single-element detector. The signal at the output of the spectrometer reads

$$S_{\parallel,\perp}(\omega) = |\tilde{E}_{\parallel,\perp}^{\mathrm{Ref}*}(\omega)|^2 + |\tilde{E}_{\parallel,\perp}^{\mathrm{FID}}(\omega)|^2 + 2\,\mathrm{Re}[\tilde{E}_{\parallel,\perp}^{\mathrm{Ref}*}(\omega)\tilde{E}_{\parallel,\perp}^{\mathrm{FID}}(\omega)\exp(i\omega\tau_d)]. \quad (2)$$

To remove the homodyne signals, which are the first two terms in Eq. (2), and measure the heterodyned term only, a shutter in the reference arm and a chopper in the signal arm were used. First, the reference signal [the first term in Eq. (2)] can be eliminated by lock-in amplifying the total FID signal (the second and third terms) chopped with subharmonic (500 Hz) frequency of the laser repetition rate (1 kHz). Then, only the homodyne FID signal (the second term) is measured by blocking the reference beam by the shutter. Finally, the heterodyne-detected spectral interferogram $S_{\parallel,\perp}^{\mathrm{het}}(\omega)$ (the last term) is obtained by subtracting the latter (homodyne FID signal) from the former (total FID signal).

Next, the standard Fourier-transformation procedure [4], which converts the measured spectral interferogram to complex electric field, was employed to ultimately obtain the complex OA susceptibility $\Delta\chi(\omega)$. First, the heterodyned spectral interferogram $S_{\parallel,\perp}^{\mathrm{het}}(\omega)$ [the last term in Eq. (2)] is inverse Fourier transformed ($F^{-1}\{S_{\parallel,\perp}^{\mathrm{het}}(\omega)\}$) and then the Heavyside step function $\theta(t)$ is multiplied to the time-domain signal ($\theta(t)F^{-1}\{S_{\parallel,\perp}^{\mathrm{het}}(\omega)\}$). The role of the Heavyside step function is to yield the complex function $\tilde{E}_{\parallel,\perp}^{\mathrm{Ref}*}(\omega)\tilde{E}_{\parallel,\perp}^{\mathrm{FID}}(\omega)\exp(i\omega\tau_d)$ when $\theta(t)F^{-1}\{S_{\parallel,\perp}^{\mathrm{het}}(\omega)\}$ is finally Fourier transformed ($F[\theta(t)F^{-1}\{S_{\parallel,\perp}^{\mathrm{het}}(\omega)\}]$). Consequently, the complex electric field $\tilde{E}_{\parallel,\perp}^{\mathrm{FID}}(\omega)$ can be obtained as

$$\tilde{E}_{\parallel,\perp}^{\mathrm{FID}}(\omega) = \frac{F[\theta(t)F^{-1}\{S_{\parallel,\perp}^{\mathrm{het}}(\omega)\}]\exp(-i\omega\tau_d)}{2\tilde{E}_{\parallel,\perp}^{\mathrm{Ref}*}(\omega)}. \quad (3)$$

This means that the FID fields $\tilde{E}_{\parallel,\perp}^{\mathrm{FID}}(\omega)$ can be completely characterized from the measured spectral interferograms $S_{\parallel,\perp}^{\mathrm{het}}(\omega)$ if one has a well-defined reference field $\tilde{E}_{\parallel,\perp}^{\mathrm{Ref}}(\omega)$ (in terms of phase and amplitude) with a fixed τ_d.

Generally, a complete characterization of the reference field is not an easy task, even if not impossible, and requires an additional measurement setup. Also, a precise determination of τ_d value within optical cycle (less than a few femtoseconds) is very difficult. Fortunately, however, the relationship of Eq. (1) indicates that there is no need to precisely characterize both $\tilde{E}_{\parallel}^{\mathrm{FID}}$ and $\tilde{E}_{\perp}^{\mathrm{FID}}$ to obtain $\Delta\chi(\omega)$ because $\Delta\chi(\omega)$ is determined by the ratio of the two complex electric fields, $\tilde{E}_{\perp}^{\mathrm{FID}}(\omega)/\tilde{E}_{\parallel}^{\mathrm{FID}}(\omega)$, which is related to the relative phase between $\tilde{E}_{\perp}^{\mathrm{FID}}(\omega)$ and $\tilde{E}_{\parallel}^{\mathrm{FID}}(\omega)$. The reference field $\tilde{E}_{\parallel,\perp}^{\mathrm{Ref}}(\omega)$ in denominator of Eq. (3) and an additional phase term $\exp(-i\omega\tau_d)$ in numerator of Eq. (3) equally contribute to both $S_{\perp}^{\mathrm{het}}(\omega)$ and $S_{\parallel}^{\mathrm{het}}(\omega)$ as long as the phase and amplitude of the electric field used and τ_d determined by the optical path difference of the interferometer are sufficiently stable and thus unchanged during the measurements of $S_{\parallel,\perp}^{\mathrm{het}}(\omega)$. Consequently, such contributions automatically cancel out when one takes the ratio of $\tilde{E}_{\perp}^{\mathrm{FID}}(\omega)$ to $\tilde{E}_{\parallel}^{\mathrm{FID}}(\omega)$.

However, it is practically difficult to measure $S_{\parallel}^{\mathrm{het}}(\omega)$ without τ_d change after the independent measurement of $S_{\perp}^{\mathrm{het}}(\omega)$. Suppose that, to measure $S_{\parallel}^{\mathrm{het}}(\omega)$, LP2, LP4, and LP0 are rotated by 90° with respect to those configuration in the cross-polarization geometry. Then, due to the large rotations of three polarizers, LP2, LP4, and LP0, the τ_d value could be substantially altered because of the changes in optical paths in the two arms of the interferometer. Consequently, the idea that LP2, LP4, and LP0 should be rotated by 90° to record $S_{\parallel}^{\mathrm{het}}(\omega)$ is not practically useful, because it causes serious phase changes in the propagating fields. Furthermore, since the electric field $\tilde{E}_{\parallel}^{\mathrm{FID}}(\omega)$ amplitude is very large in such a case, the problem of dynamic range of detector makes full $\tilde{E}_{\parallel}^{\mathrm{FID}}(\omega)$ signal detection difficult. Thus, we used a different and practically useful trick. Simply, we slightly rotated the LP1 by about 0.5° and fixed all the other polarizers. Despite this small opening of the polarizer to allow a little amount of $\tilde{E}_{\parallel}^{\mathrm{FID}}(\omega)$ to pass through it, the dominant contribution is still from $\tilde{E}_{\parallel}^{\mathrm{FID}}(\omega)$. This technique has notable advantages: (1) optical components and experimental setup are minimally altered, (2) the dynamic range problem of the detector can be overcome by reducing the signal field amplitude, and (3) a little change in LP1 angle guarantees τ_d change to be negligibly small. All these aspects were experimentally confirmed. By combining Eqs. (1) and (3), the complex OA susceptibility $\Delta\chi(\omega)$ could be finally obtained as

$$\Delta\chi(\omega) = \frac{cn(\omega)}{\pi\omega L}\frac{F[\theta(t)F^{-1}\{S_{\perp}^{\mathrm{het}}(\omega)\}]}{F[\theta(t)F^{-1}\{S_{\parallel}^{\mathrm{het}}(\omega)\}]}. \tag{4}$$

It is this equation that can be used to convert the measured spectral interferograms to the OA susceptibility.

C. Absolute VCD and VORD Values

For a variety of applications, it is important to determine the absolute VCD and VORD values, not just their spectral line shapes, from the VOAFID measurements. Here, we show that such quantitative measurement of the VCD and VORD is possible with the current technique. From the definition of the absorption coefficient [19], the difference between the two absorption coefficients of chiral molecules for LCP and RCP beams, $\Delta\kappa_a(\omega)$, is given as

$$\Delta\kappa_a(\omega) = \frac{4\pi\omega}{n(\omega)c}\mathrm{Im}[\Delta\chi(\omega)]. \tag{5}$$

Since the absorbance is defined by common logarithms of the intensity ratio between incident and transmitted beams, the differential absorbance ΔA (VCD) is given as

$$\Delta A(\omega) = \frac{\Delta\kappa_a(\omega)L}{2.303} = \frac{4}{2.303}\mathrm{Im}\left[\frac{F[\theta(t)F^{-1}\{S_{\perp}^{\mathrm{het}}(\omega)\}]}{F[\theta(t)F^{-1}\{S_{\parallel}^{\mathrm{het}}(\omega)\}]}\right]. \tag{6}$$

On the other hand, the optical rotation angle $\Delta\varphi(\omega)$ caused by the circular birefringence is defined as the half of phase difference between LCP and RCP after passing through the sample. Because $1+4\pi\chi'_{L,R}(\omega) \gg 4\pi\chi''_{L,R}(\omega)$, where $\chi'_{L,R}(\omega)$ and $\chi''_{L,R}(\omega)$ are the real and imaginary parts of the linear susceptibilities for LCP and RCP lights, respectively, the indices of refraction of LCP and RCP beams are given by $n_{L,R}(\omega)=[1+4\pi\chi'_{L,R}(\omega)]^{1/2}$ and thus $n_L^2(\omega)-n_R^2(\omega)=4\pi\,\mathrm{Re}[\Delta\chi(\omega)]$. Then, the circular birefringence $\Delta n(\omega)=n_L(\omega)-n_R(\omega)$ can be expressed as

$$\Delta n(\omega) = \frac{2\pi}{n(\omega)}\mathrm{Re}[\Delta\chi(\omega)]. \tag{7}$$

By combining Eqs. (7) and (4), the optical rotation angle is thus given as

$$\Delta\varphi(\omega) \equiv \Delta n(\omega)\frac{\omega}{2c}L = \mathrm{Re}\left[\frac{F[\theta(t)F^{-1}\{S_{\perp}^{\mathrm{het}}(\omega)\}]}{F[\theta(t)F^{-1}\{S_{\parallel}^{\mathrm{het}}(\omega)\}]}\right]. \tag{8}$$

However, it is noted that the results in Eqs. (6) and (8) are not directly relevant in the present case, because we measured only a partial amount of $\tilde{E}_{\parallel}^{\mathrm{FID}}(\omega)$ by rotating LP1 by $\delta_{\parallel}$ (=0.5°) angle for the measurement of $S_{\parallel}^{\mathrm{het}}(\omega)$. Hence, from Malus law, Eqs. (6) and (8) should be rewritten as

$$\Delta A(\omega,\delta_{\parallel}) = \frac{4}{2.303}\mathrm{Im}\left[\frac{F[\theta(t)F^{-1}\{S_{\perp}^{\mathrm{het}}(\omega)\}]}{F[\theta(t)F^{-1}\{S_{\parallel}^{\mathrm{het}}(\omega,\delta_{\parallel})\}]}\right]\sin\,\delta_{\parallel}, \tag{9}$$

$$\Delta\varphi(\omega,\delta_{\parallel}) = \mathrm{Re}\left[\frac{F[\theta(t)F^{-1}\{S_{\perp}^{\mathrm{het}}(\omega)\}]}{F[\theta(t)F^{-1}\{S_{\parallel}^{\mathrm{het}}(\omega,\delta_{\parallel})\}]}\right]\sin\,\delta_{\parallel}, \tag{10}$$

where $\delta_{\parallel}$ is the LP1 angle deviated from the cross-polarization geometry and $S_{\parallel}^{\mathrm{het}}(\omega,\delta_{\parallel})$ is the spectral interferogram at $\delta_{\parallel}$ angle.

3. RESULTS

A. VCD and VORD Measurements

To demonstrate the experimental feasibility, we carried out the VOAFID measurements of two small organic molecules, (R)-limonene and (1S)-β-pinene, diluted in carbon tetrachloride (CCl_4). Figure 2 depicts the step-by-step procedure for retrieving the VCD and VORD spectra from the measured spectral interferograms $S_{\perp}^{\mathrm{het}}(\omega)$ (solid curve) and $S_{\parallel}^{\mathrm{het}}(\omega)$ (dashed curve) in Fig. 2(a). Although the pulse spectrum [full width at half maximum (FWHM) ~ 270 cm^{-1}] is broader than the spectral window shown in Fig. 2(a) (strong dichroic region of the calcite plate), we can ignore the spectral interferogram outside of the spectrally working region of the calcite polarizer [3]. The measured spectral interferograms $S_{\parallel,\perp}^{\mathrm{het}}(\omega)$ were then inverse Fourier transformed and multiplied by the Heavyside step function, and the resultant time-domain signal amplitudes, $|\theta(t)F^{-1}\{S_{\perp}^{\mathrm{het}}(\omega)\}|$ (solid curve) and $|\theta(t)F^{-1}\{S_{\parallel}^{\mathrm{het}}(\omega)\}|$ (dashed curve), are plotted in Fig. 2(b). In practice, we used $\theta(t-0.5\ \mathrm{ps})$ instead of $\theta(t)$ in order to remove the residual homodyne and dc signals included in $S_{\parallel,\perp}^{\mathrm{het}}(\omega)$, which appear at time zero [shaded area in Fig. 2(b)] in the time-domain FID field. Finally, the VCD (solid line) and VORD (dashed line) spectra could be

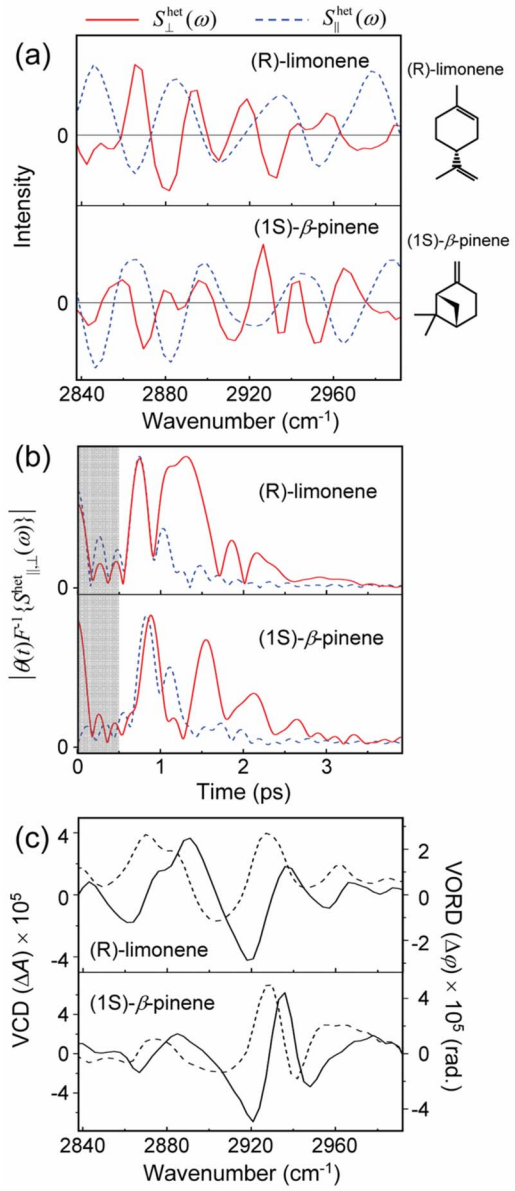

Fig. 2. (Color online) VCD and VORD measurements of (R)-limonene (upper panel in each figure) and (1S)-β-pinene (lower panel) in CCl_4 using the FTSI method. (a) Experimentally measured heterodyne-detected spectral interferograms, $S_{\perp}^{het}(\omega)$ (solid curve) and $S_{\parallel}^{het}(\omega)$ (dashed curve), which were properly factorized for comparison. (b) Normalized amplitudes of the time-domain signal, $|\theta(t)F^{-1}\{S_{\perp}^{het}(\omega)\}|$ (solid curve) and $|\theta(t)F^{-1}\{S_{\parallel}^{het}(\omega)\}|$ (dashed curve). The residual homodyne and dc signals near time zero (shaded area) is excluded by multiplying $\theta(t-0.5\ \text{ps})$ to $F^{-1}\{S_{\parallel,\perp}^{het}(\omega)\}$ instead of $\theta(t)$. (c) VCD (solid curve, left scale) and VORD (dashed curve, right scale) spectra obtained by using Eqs. (9) and (10), respectively.

simultaneously retrieved by using Eqs. (9) and (10), respectively, and are depicted in Fig. 2(c). Not only the spectral characteristic of each individual VCD spectrum but also their absolute VCD values are consistent with the previous data obtained with cw FT-IR VCD spectrometer [20]. This indicates that our femtosecond VOA measurement setup and the retrieval process of VCD and VORD spectra discussed above are quite stable and reliable.

B. Light Intensity and Phase Fluctuations: Simulation

The optical activity signals (CD and ORD) obtained by using the present OAFID measurement technique are expected to be much less vulnerable to the incident light intensity fluctuation in comparison with the differential CD measurement technique, but sensitive to the τ_d fluctuation (phase fluctuation) because the method relies on the interferometric detection. To examine these fluctuation effects, we carried out numerical simulation studies of the VOAFID measurement for the same theoretical model system as that reported before [2]. The parameters used are summarized in Table 1. Essentially, the model system consists of three IR- and VCD-active modes. Their vibrational frequencies, transition dipole strengths, and rotational strengths are given in Table 1. For the numerical simulations, the reference pulse for the heterodyne detection is assumed to have Gaussian temporal envelop with the FWHM of 100 fs (intensity profile) and the center frequency of 2950 cm^{-1}. We deliberately considered both perfect and imperfect cross-polarization detection geometries in order to mimic the experimental situations and studied whether the phase sensitive retrieval of VCD spectrum is feasible or not in the presence of large achiral contributions. For clarity, two parameters, $\delta_{\parallel}$ and $\delta_{\perp}$, corresponding to the angles deviated from the cross-polarization geometry between LP1 and LP2 need to be assigned: $\delta_{\parallel}$ (0.5° for the real experiment) is considered to be the controllable parameter for the measurement of the parallel-detected spectral interferogram $S_{\parallel}^{het}(\omega)$ as described in Sec. 2, whereas $\delta_{\perp}$ is that for the perpendicular-detected spectral interferogram $S_{\perp}^{het}(\omega)$. For perfect and imperfect polarizers, $\delta_{\perp}$ angles were set to 0° and 0.05°, respectively.

For the present numerical simulation, it was assumed that a train of input pulses entering the Mach-Zehnder interferometer has finite intensity fluctuation and thus the amplitudes of $\tilde{E}_{\parallel,\perp}^{Ref}(\omega)$ and $\tilde{E}_{\parallel,\perp}^{FID}(\omega)$ fluctuate synchronously with Gaussian statistics. Also, the fluctuations are not frequency dependent, so that the spectral line shape of every fluctuating electric field remains the same, and any other fluctuation source is not taken into consideration. Although the above simulation conditions appear to be too simple to describe complicated fluctuation phenomena occurring in a real experiment, it certainly helps to separately study specific effects from a given fluctuation source on the measurement. For the sake of simplicity, the measurement method in the present simulation is assumed to be made by a multichannel array detector, which enables simultaneous detection of the entire fre-

Table 1. Simulation Parameters Used for Obtaining VCD Spectrum from the VOAFID Measurement via the FTSI for a Model System with Three Vibrational Modes [2]

	Mode 1	Mode 2	Mode 3
Center frequency (cm^{-1})	2900	2950	3000
Dephasing rate (fs^{-1})	0.006	0.004	0.004
Transition dipole strength[a]	1	0.5	0.3
Rotational strength[a]	-5×10^{-5}	2.5×10^{-5}	-1.5×10^{-5}

[a]Values represent the relative strengths.

quency components of the electric field, instead of frequency-scanning method. The signal averaging is performed for 100 pulse measurements and corresponding spectral interferograms. As the standard deviation of intensity fluctuation was varied from 0% to 50% from its average value, the heterodyne-detected spectral interferograms with this intensity noise were converted to the VCD spectra by using Eq. (9) and they are plotted in Figs. 3(a) and 3(b). It is clearly shown that the retrieved VCD spectra have sufficiently good signal-to-noise ratio even with intensity fluctuation of 50% in both cases of $\delta_\perp = 0°$ (perfect polarizer) and $\delta_\perp = 0.05°$ (imperfect polarizer). For comparison, we also carried out another simulation for the conventional differential measurement and depict the result in Fig. 3(c). It shows that the same level of VCD signal ($\Delta A \sim 10^{-5}$) cannot be discriminated from the large achiral intensity fluctuation until much higher light stability (<0.01% fluctuation) than the above case (VOAFID) is reached. This demonstrates that the VOAFID measurement, where the measured value at a time is ΔA itself, is less influenced by the intensity fluctuation than the differential one.

Nevertheless, since the present method relies on the spectral interferometry, where two electric fields, i.e., FID and reference, are separated by a fixed time delay τ_d and detected in the frequency domain, the measured spectral interferograms are subject to the τ_d change caused by the fluctuation of the optical path difference between the two arms of the interferometer. If the τ_d fluctuation is the only source of noise, the spectral interferograms can be expressed as

$$S_{\parallel,\perp}^{\text{het}}(\omega) = 2\,\text{Re}[\tilde{E}_{\parallel,\perp}^{\text{Ref}*}(\omega)\tilde{E}_{\parallel,\perp}^{\text{FID}}(\omega)\exp\{i\omega(\tau_d + \delta\tau_d)\}], \quad (11)$$

where $\delta\tau_d$ denotes the deviation of the delay time from the mean value τ_d. Due to the resultant phase fluctuation, the spectral interferogram fluctuates too. The simulation condition is the same as that described above and the amount of τ_d fluctuation is specified by the standard deviation of one period (11.3 fs) of the IR field with the frequency of 2950 cm^{-1}. Figure 4 shows the simulated VCD spectra obtained at various standard deviations. If the polarizers are perfect, which corresponds to the case $\delta_\perp = 0°$, the retrieved VCD spectra are fairly good even in the case that the standard deviation $\langle \delta\tau_d^2 \rangle^{1/2}$ is 30% of 11.3 fs.

On the other hand, if the polarizers are not perfect, the added large achiral contribution significantly increases the noise level, which is caused by the phase fluctuation. Note that the retrieved VCD spectrum at $\delta_\perp = 0.05°$ appears to be quite noisy in comparison to that at $\delta_\perp = 0°$ (compare the cases with 1% standard deviation). However, it was found that our experimental setup is sufficiently stable with respect to the τ_d fluctuation during the data collection time (~tens of minutes).

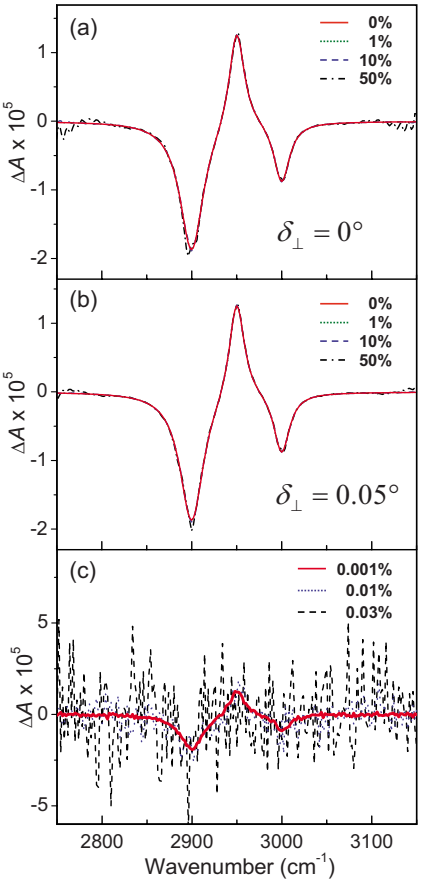

Fig. 3. (Color online) VCD spectra simulated by using the present method at (a) $\delta_\perp = 0°$ (optically perfect) and (b) $\delta_\perp = 0.05°$ (optically imperfect) in the presence of light source fluctuation only. The VCD spectrum obtained by using the differential measurement method is shown in (c). Values in % in this figure denote the standard deviation of the fluctuating pulse-to-pulse intensity.

C. Phase Sensitive Detection: Experimental Verification

The theoretical result in Eq. (1) is valid only when the polarizers (LP1 and LP2) are perfect. However, if they are

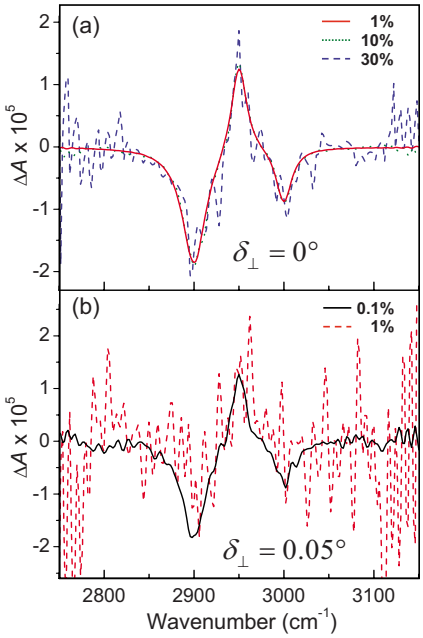

Fig. 4. (Color online) VCD spectra simulated by using the present method at (a) $\delta_\perp = 0°$ (optically perfect) and (b) $\delta_\perp = 0.05°$ (optically imperfect) in the presence of phase fluctuation only. Values in % denote the standard deviation of the fluctuating delay time around one period (11.3 fs) of the center frequency (2950 cm^{-1}) of the reference pulse.

not, the achiral FID field cannot be completely rejected by LP2 and consequently the partially leaked achiral signal would be detected together with the chiral field. Therefore, its contribution should be added to the right-hand side of Eq. (1) and consequently $\tilde{E}^{\mathrm{FID}}_{\perp,\mathrm{imperfect}}(\omega)$, under optically imperfect condition, can be rewritten as

$$\tilde{E}^{\mathrm{FID}}_{\perp,\mathrm{imperfect}}(\omega) = \frac{\pi\omega L}{cn(\omega)}\Delta\chi(\omega)\tilde{E}^{\mathrm{FID}}_{\parallel}(\omega) + \rho^{1/2}\tilde{E}^{\mathrm{FID}}_{\parallel}(\omega), \tag{12}$$

where the second term represents the transmitted electric field (not intensity) through the imperfect LP2 polarizers and $\rho^{1/2}$ determines the magnitude of the leaked achiral field. As the extinction ability of the polarizer gets worse (larger ρ value), the first term (chiral FID) on the right-hand side of Eq. (12) becomes significantly masked by the second term (achiral FID). However, the VCD signal ($\propto \mathrm{Im}[\Delta\chi(\omega)]$) is phase shifted by 90° from $\tilde{E}^{\mathrm{FID}}_{\parallel}(\omega)$, so that the phase-sensitive detection of VCD signal is in principle possible. To examine the contribution of the second term (achiral FID) in more detail, Eq. (12) can be rewritten as

$$\tilde{E}^{\mathrm{FID}}_{\perp,\mathrm{imperfect}}(\omega) = \frac{\pi\omega L}{cn(\omega)}\Delta\chi_{\mathrm{imperfect}}(\omega)\tilde{E}^{\mathrm{FID}}_{\parallel}(\omega), \tag{13}$$

where

$$\Delta\chi_{\mathrm{imperfect}}(\omega) = \{\mathrm{Re}[\Delta\chi(\omega)] + \gamma\} + i\ \mathrm{Im}[\Delta\chi(\omega)]. \tag{14}$$

Here, i is the imaginary number and $\gamma=(cn/\pi\omega L)\rho^{1/2}$. Because ρ is real, $\mathrm{Re}[\Delta\chi_{\mathrm{imperfect}}(\omega)] \equiv \mathrm{Re}[\Delta\chi(\omega)]+\gamma$ and $\mathrm{Im}[\Delta\chi_{\mathrm{imperfect}}(\omega)] \equiv \mathrm{Im}[\Delta\chi(\omega)]$. This means that the achiral background contribution ($\rho^{1/2}\tilde{E}^{\mathrm{FID}}_{\parallel}$), which is a noise in this case, does not affect the imaginary part of $\Delta\chi_{\mathrm{imperfect}}(\omega)$ but contributes only to its real part as a background offset (γ). Note that the numerical simulation study already showed that the VCD spectrum can be reliably obtained from Eq. (9) under the optically imperfect condition ($\delta_\perp=0.05°$) as long as the interferometer is sufficiently stable with respect to the phase fluctuation [see Fig. 4(b)].

To verify whether such a phase sensitive detection is also experimentally feasible or not, the VOAFID measurement of (1S)-β-pinene in CCl_4 was performed. For mimicry of optically imperfect conditions, the leaking level of achiral signal was controlled by varying $\delta_\perp$ from 0.005° to 0.05°. As $\delta_\perp$ increases, ρ becomes larger and therefore the achiral contribution ($\rho^{1/2}\tilde{E}^{\mathrm{FID}}_{\parallel}$) increases. The measured spectral interferograms $S^{\mathrm{het}}_{\parallel,\perp}(\omega)$ for varying $\delta_\perp$ values are plotted in Fig. 5(a). Note that the calcite polarizer ($\rho<10^{-9}$) used here is nearly perfect for the present case and $S^{\mathrm{het}}_{\perp}(\omega)$ measured at finite $\delta_\perp$ originates from $\tilde{E}^{\mathrm{FID}}_{\perp,\mathrm{imperfect}}(\omega)$ in Eq. (12). At $\delta_\perp=0°$, it is clearly shown that $S^{\mathrm{het}}_{\perp}(\omega)$ (solid curve) and $S^{\mathrm{het}}_{\parallel}(\omega)$ (dashed curve) have distinctively different spectral phases and amplitudes with respect to each other and this confirms that they originate from the chiral and achiral FID fields, respectively. However, as $\delta_\perp$ increases, distinctive features of $S^{\mathrm{het}}_{\perp}(\omega)$ at $\delta_\perp=0°$ disappear due to the substantial contribution from the achiral signal and $S^{\mathrm{het}}_{\perp}(\omega)$ becomes nearly the same with $S^{\mathrm{het}}_{\parallel}(\omega)$ at $\delta_\perp=0.05°$. This indicates

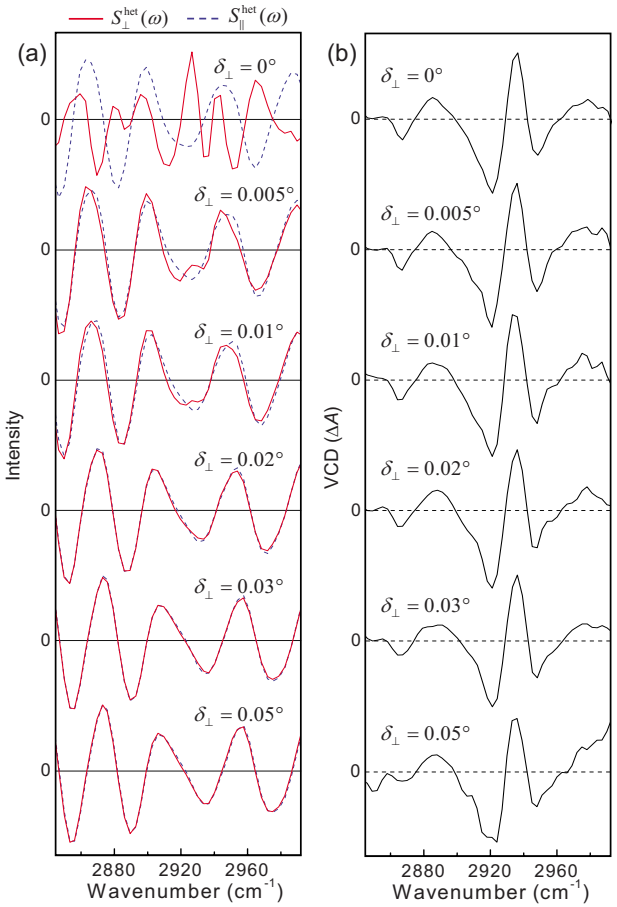

Fig. 5. (Color online) (a) Normalized heterodyned spectral interferograms, $S^{\mathrm{het}}_{\perp}$ (solid curve) and $S^{\mathrm{het}}_{\parallel}$ (dashed curve), measured in the C-H stretch vibration region of (1S)-β-pinene in CCl_4 at various $\delta_\perp$ angles. (b) VCD spectra retrieved by Eq. (9) at each $\delta_\perp$ angle. All the VCD spectra were corrected by each individual linear offset base line for a clear comparison.

that most of the perpendicular-detected FID field $\tilde{E}^{\mathrm{FID}}_{\perp,\mathrm{imperfect}}(\omega)$ in this case of $\delta_\perp=0.05°$ is mainly represented by the achiral contribution [second term of Eq. (12)].

However, it is interesting that all the converted spectra with Eq. (9) depicted in Fig. 5(b) exhibit the same characteristic VCD spectral features associated with the C-H stretch vibration of (1S)-β-pinene [20]. That is to say, the VCD spectra could be reliably retrieved even when the weak chiral signal is almost completely masked by large achiral background (particularly see the lower three cases in Fig. 5). This implies that the phase sensitive extraction of the VCD spectrum is experimentally feasible even though the polarizer is not entirely perfect.

To gain a more insight into the retrieval process implemented in such an imperfect polarization condition, we plot the real and imaginary part spectra, obtained by Eqs. (10) and (9) from $S^{\mathrm{het}}_{\parallel,\perp}(\omega)$ in Fig. 5(a), in the upper and lower panels of Fig. 6, respectively. All the real part spectra at various $\delta_\perp$ angles have almost identical spectral shapes (peak position, phase, and relative amplitude), but they are simply different from one another by constant offsets. The larger $\delta_\perp$ angle is, the larger the offset magnitude is. In contrast, the imaginary spectra do not sig-

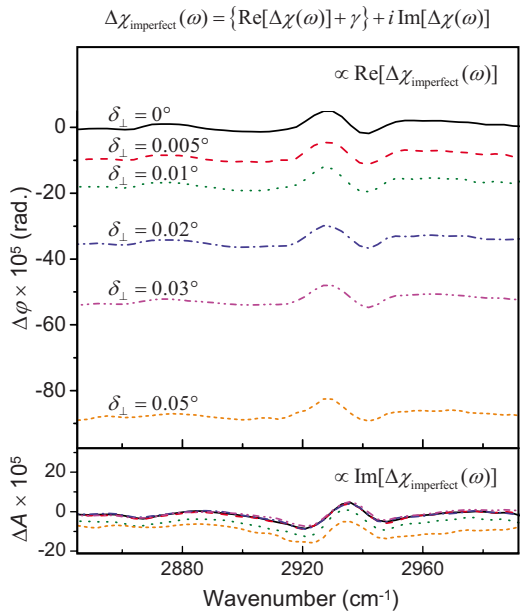

Fig. 6. (Color online) Real (upper panel, VORD) and imaginary (lower panel, VCD, not base-line-corrected) part spectra obtained by Eqs. (9) and (10) under optically imperfect conditions. As $\delta_\perp$ angle increases, the extinction ratio (ρ) of the polarizers becomes larger and consequently the offset magnitude of $\text{Re}[\Delta\chi_{\text{imperfect}}(\omega)]$ increases together, whereas the imaginary part spectra are not affected by $\delta_\perp$ angle because $\text{Im}[\Delta\chi_{\text{imperfect}}(\omega)] = \text{Im}[\Delta\chi(\omega)]$.

nificantly depend on $\delta_\perp$. These features are consistent with the fact that $\text{Re}[\Delta\chi_{\text{imperfect}}(\omega)]$ is given by the sum of $\text{Re}[\Delta\chi(\omega)]$ proportional to the VORD and constant offset γ, whereas $\text{Im}[\Delta\chi_{\text{imperfect}}(\omega)]$ is given by $\text{Im}[\Delta\chi(\omega)]$ itself that is directly related to the VCD.

4. DISCUSSION

Although cw FT-IR VCD spectrometers are commercially available, the data collection time for obtaining a VCD spectrum with good signal-to-noise ratio is usually very long. For example, it takes a few hours to measure a VCD spectrum for the amide I vibrations of small peptide, of which rotational strength is about five times larger than that of C-H stretch vibration of limonene or β-pinene [21,22]. In the present method, however, by virtue of optical amplification with a heterodyne-detection scheme as well as by the advantages of the nondifferential detection scheme, the data collection time required for measuring a VCD spectrum with a sufficient signal-to-noise ratio could be dramatically reduced. To obtain the spectral interferogram shown in Fig. 2(a), ~50 data points were acquired by scanning the monochromator and each data point was averaged with 100 ms time constant of lock-in amplifier during one monochromator scan, and this scan was repeated ten times for further averaging when measuring a single $S_\perp^{\text{het}}(\omega)$ [single scan for the measurement of $S_\parallel^{\text{het}}(\omega)$]. Consequently, it took just about 10 min to measure the VCD spectra with excellent signal-to-noise ratio as shown in Fig. 2(c). If we used a multichannel array detector, which enables one to simultaneously detect the entire frequency components and/or if the repetition rate of the IR laser (1 kHz) was increased, the data collection time would have been further reduced to subsecond time scale by saving the monochromator-scanning and the signal-settling times.

The conventional VORD measurement experiments have been performed previously, but they are the cases of liquid crystal [23] that has well-defined directionality and thus shows extremely large chiral effect ($\Delta\varphi \sim 7000$ grad/mm) and of off-resonant measurement [24] where the use of much thicker sample is possible—note that there is no attenuation of incident beam intensity due to the nonresonance condition. Thus, the resonant VORD measurement of a small chiral molecule in solution has been considered to be quite challenging not only because of its small optical rotation but also because of a large intensity attenuation in the resonant frequency range, so that (to the authors' knowledge) it has not been carried out before. However, as clearly demonstrated in the present work, we showed that, by simply taking the real part of $\Delta\chi(\omega)$, the resonant VORD signal as small as about 10^{-5} rad can be successfully measured [see Fig. 2(c)].

One of the most important applications and immediate concerns is the extension of the present technique to time-resolved measurements. The time-resolved CD or VCD experiment can provide crucial information on the structural evolution of biomolecules or chemical reaction dynamics involving chiral molecules. From Kliger's approach based on the ellipsometric detection technique [25,26], nanosecond CD measurements could be achieved but its time resolution limit set by the speed of electronics made it difficult to directly follow much faster dynamics ranging from femtoseconds to picoseconds. As an alternative approach, Xie and Simon [27–29] combined a picosecond pulsed laser with an electro-optic modulator to measure the picosecond CD changes. However, since it is based on a differential measurement with sequentially alternating LCP and RCP pulses (polarization modulation), their fluctuations (LCP and RCP) can significantly deteriorate the small CD signal given by the difference between them [see Fig. 3(c)]. Therefore, in the case of VCD ($\Delta A = 10^{-4} - 10^{-5}$) measurement, such a weak chiral signal is likely to be very difficult to detect with standard laser stability (0.1%) and measurement scheme. Bonmarin and Helbing [30] resolved this problem by simply adding a reference detector that compensates the pulse fluctuations and succeeded in the picosecond time-resolved VCD measurement. On the other hand, the present method, where every VOAFID including the entire VCD information is measured and then averaged, is proven to be much less sensitive to the light intensity fluctuation (see Fig. 3), so that no intensity reference is needed. But, it is slightly affected by the phase fluctuation caused by the external perturbations such as air flow and/or acoustic noise because it relies on the interferometric detection (see Fig. 4). Nevertheless, such an obstacle can be overcome by employing an active phase-locking technique in the future.

An important technical issue in the pump-probe-type time-resolved CD experiments is about how sensitive the method is to pump-induced changes. Conventionally, the time-resolved CD trace is obtained by directly differentiating the CD signals at different pump-probe delay times. Because the pump-induced changes are typically much

smaller than the weak static CD signal, the measured signal is inevitably quite noisy. Therefore, a pump modulation for increased sensitivity would be required to detect such a small CD change only. On the other hand, the present method does not require such polarization modulations of the probe pulse and consequently the pump modulation can be easily introduced in a time-resolved CD experiment. It is believed that this could be a dramatic advantage of the present phase sensitive detection method.

Recently, a highly relevant experimental method using a similar cross-polarization detection scheme was proposed and its feasibility was demonstrated. By using a combination of a pair of crossed polarizers and Babinet-Soleil compensator, Niezborala and Hache [31,32] could successfully introduce a pump modulation in their pump-probe electronic CD (not vibrational CD) experiment and obtained improved time-resolved CD and ORD traces. This is an outstanding achievement that demonstrates time-resolved measurements of electronic OA for the cases that the rotational strengths (CD intensity) are large. Their approach appears to be geometrically similar to the present method, but their method is to measure output intensity, whereas we measured the complex electric fields at the amplitude level. Therefore, their signal is not phase sensitive and does not contain complete information on chirality (e.g., handedness). Thus, transient CD or ORD had to be obtained by individually scanning the retardation or analyzer angle at a given frequency. In our method, however, the direct heterodyne detection of chiral electric field enables one not only to measure CD and ORD simultaneously but also to obtain the whole spectra without frequency scan of the input pulse as long as the pulse spectrum is broad enough to cover the vibrations of interest.

Despite our successful measurements of the VOAFID fields for small chiral molecules, unfortunately, the working spectral window of the calcite polarizer is rather narrow and limited to the C-H stretch vibration region ($2830-3000\ cm^{-1}$). For a wide range of IR applications, it will be necessary to have polarizers with $\rho < 10^{-9}$ over the broader IR frequency range, but such polarizers are not commercially available at the moment. However, we are currently developing a new experimental technique to overcome such limitations and the results will be reported elsewhere.

5. SUMMARY

The cross-polarization detection methods enables one to remove the large achiral background signal and to selectively measure the OAFID field containing the entire linear OA information of the chiral sample under investigation. Due to the coupling between the chiral and achiral FID fields, however, the parallel-polarized component must also be measured to obtain a complete form of the complex OA susceptibility. It turned out that the susceptibility is linearly proportional to the ratio of the mutually orthogonal FID fields. The spectral interferometric heterodyne detection of these FID fields makes it possible not only to enhance the weak chiral signal field but also to determine their relative phases and amplitudes. To minimize any phase change introduced during separate parallel and perpendicular measurements, we slightly rotated the input polarizer (LP1) from the ideal cross-polarization geometry to measure the parallel component, which is the achiral electric dipole FID. Consequently, the VCD and VORD spectra of small chiral molecules, (R)-limonene and (1S)-β-pinene in CCl_4, were successfully measured. From the numerical simulation studies, it was found that the present method is robust to the light source fluctuation, but rather sensitive to the phase fluctuation. Also, it was shown that the VCD spectrum could be reliably retrieved even in the presence of large achiral contributions as long as the phase stability of the interferometer is acceptable. To experimentally demonstrate the feasibility of phase sensitive detection of VCD signal, we deliberately carried out the VOAFID measurement experiments of (1S)-β-pinene in CCl_4 under the optically imperfect conditions and found that even the VCD signal contaminated by much larger achiral background signal could be separately measured by using the present FTSI procedure. Finally, a discussion on the extension of the present technique to time-resolved measurements was presented.

In the present work, we demonstrated that the VCD and VORD spectra of chiral molecules can be experimentally measured by using the heterodyne-detected spectral interferometry method utilizing a femtosecond IR pulse. However, the same principle and methodology can be used to measure electronic CD and ORD spectra, even though the linear polarizers, optics, and detector should be replaced with appropriate ones for a femtosecond UV-vis pulse. Currently, we are constructing such an electronic optical activity measurement setup and will present experimental results elsewhere. Thus, we anticipate that this technique based on the FTSI measurement of OAFID field will be of critical use in studying various chemical and biological processes involving changes in molecular chiralities in condensed phases.

ACKNOWLEDGMENTS

This work was supported by the Creative Research Initiatives (CMDS) of MEST/KOSEF for M.C., KBSI grant T29720 for S.J.J., and Basic Research Promotion grant 2008-331-C00134 of MEST/KOSEF for Z.H.K.

REFERENCES

1. *Circular Dichroism: Principles and Applications*, edited by N. Berova, K. Nakanishi, and R. W. Woody (Wiley-VCH, 2000).
2. H. Rhee, J.-H. Ha, S.-J. Jeon, and M. Cho, "Femtosecond spectral interferometry of optical activity: theory," J. Chem. Phys. **129**, 094507 (2008).
3. H. Rhee, Y.-G. June, J.-S. Lee, K.-K. Lee, J.-H. Ha, Z. H. Kim, S.-J. Jeon, and M. Cho, "Femtosecond characterization of vibrational optical activity of chiral molecules," Nature **458**, 310–313 (2008).
4. L. Lepetit, G. Cheriaux, and M. Joffre, "Linear techniques of phase measurement by femtosecond spectral interferometry for applications in spectroscopy," J. Opt. Soc. Am. B **12**, 2467–2474 (1995).
5. D. N. Fittinghoff, J. L. Bowie, J. N. Sweetser, R. T. Jennings, M. A. Krumbugel, K. W. DeLong, R. Trebino, and I. A. Walmsley, "Measurement of the intensity and phase of

ultraweak, ultrashort laser pulses," Opt. Lett. **21**, 884–886 (1996).
6. W. J. Walecki, D. N. Fittinghoff, A. L. Smirl, and R. Trebino, "Characterization of the polarization state of weak ultrashort coherent signals by dual-channel spectral interferometry," Opt. Lett. **22**, 81–83 (1997).
7. A. Albrecht Ferro, J. D. Hybl, and D. M. Jonas, "Complete femtosecond linear free induction decay, Fourier algorithm for dispersion relations, and accuracy of the rotating wave approximation," J. Chem. Phys. **114**, 4649–4656 (2001).
8. M. T. Zanni, N.-H. Ge, Y. S. Kim, and R. M. Hochstrasser, "Two-dimensional IR spectroscopy can be designed to eliminate the diagonal peaks and expose only the crosspeaks needed for structure determination," Proc. Natl. Acad. Sci. U.S.A. **98**, 11265–11270 (2001).
9. M. Khalil, N. Demirdoven, and A. Tokmakoff, "Coherent 2D IR spectroscopy: molecular structure and dynamics in solution," J. Phys. Chem. A **107**, 5258–5279 (2003).
10. T. Brixner, J. Stenger, H. M. Vaswani, M. Cho, R. E. Blankenship, and G. R. Fleming, "Two-dimensional spectroscopy of electronic couplings in photosynthesis," Nature **434**, 625–628 (2005).
11. T. H. Zhang, C. N. Borca, X. Li, and S. T. Cundiff, "Optical two-dimensional Fourier transform spectroscopy with active interferometric stabilization," Opt. Express **13**, 7432–7441 (2005).
12. S.-H. Lim, A. G. Caster, and S. R. Leone, "Fourier transform spectral interferometric coherent anti-Stokes Raman scattering (FTSI-CARS) spectroscopy," Opt. Lett. **32**, 1332–1334 (2007).
13. M. Cho, H. M. Vaswani, T. Brixner, J. Stenger, and G. R. Fleming, "Exciton analysis in 2D electronic spectroscopy," J. Phys. Chem. B **109**, 10542–10556 (2005).
14. D. J. Kane and R. Trebino, "Characterization of arbitrary femtosecond pulses using frequency-resolved optical gating," IEEE J. Quantum Electron. **29**, 571–579 (1993).
15. C. Iaconis and I. A. Walmsley, "Spectral phase interferometry for direct electric-field reconstruction of ultrashort optical pulses," Opt. Lett. **23**, 792–794 (1998).
16. R. Loudon, *The Quantum Theory of Light* (Oxford University Press, 1983).
17. T. J. Bridges and J. W. Kluver, "Dichroic calcite polarizers for the infrared," Appl. Opt. **4**, 1121–1125 (1965).
18. E. Hecht, *Optics* (Addison-Wesley Longman, 1998).
19. S. Mukamel, *Principles of Nonlinear Optical Spectroscopy* (Oxford University Press, 1995).
20. C. Guo, R. D. Shah, R. K. Dukor, T. B. Freedman, X. Cao, and L. A. Nafie, "Fourier transform vibrational circular dichroism from 800 to 10,000 cm^{-1}: near-IR-VCD spectral standards for terpenes and related molecules," Vib. Spectrosc. **42**, 254–272 (2006).
21. K.-K. Lee, S. Hahn, K.-I. Oh, J. S. Choi, C. Joo, H. Han, and M. Cho, "Structure of N-acetylproline amide in liquid water: experimentally measured and numerically simulated infrared and vibrational circular dichroism spectra," J. Chem. Phys. **110**, 18834–18843 (2006).
22. K.-K. Lee, K.-I. Oh, H. Lee, C. Joo, H. Han, and M. Cho, "Dipeptide structure determination by vibrational circular dichroism combined with quantum chemistry calculations," ChemPhysChem **8**, 2218–2226 (2007).
23. V. B. Schrader and E. H. Korte, "Infrarot-rotationsdispersion (IRD)," Angew. Chem. **84**, 218–219 (1972).
24. Y. N. Chirgadze, S. Y. Venyaminov, and V. M. Lobachev, "Optical rotatory dispersion of polypeptides in the near-infrared region," Biopolymers **10**, 809–820 (1971).
25. J. W. Lewis, R. F. Tilton, C. M. Einterz, S. J. Milder, I. D. Kuntz, and D. S. Kliger, "New technique for measuring circular dichroism changes on a nanosecond time scale: Application to (carbonmonoxy)myoglobin and (carbonmonoxy)hemoglobin," J. Phys. Chem. **89**, 289–294 (1985).
26. R. A. Goldbeck, D. B. Kim-Shapiro, and D. S. Kliger, "Fast natural and magnetic circular dichroism spectroscopy," Annu. Rev. Phys. Chem. **48**, 453–479 (1997).
27. X. Xie and J. D. Simon, "Picosecond time-resolved circular dichroism spectroscopy: experimental details and applications," Rev. Sci. Instrum. **60**, 2614–2627 (1989).
28. X. Xie and J. D. Simon, "Picosecond circular dichroism spectroscopy: a Jones matrix analysis," J. Opt. Soc. Am. B **7**, 1673–1684 (1990).
29. X. Xie and J. D. Simon, "Picosecond time-resolved circular dichroism study of protein relaxation in myoglobin following photodissociation of CO," J. Am. Chem. Soc. **112**, 7802–7803 (1990).
30. M. Bonmarin and J. Helbing, "A picosecond time-resolved vibrational circular dichroism spectrometer," Opt. Lett. **33**, 2086–2088 (2008).
31. C. Niezborala and F. Hache, "Measuring the dynamics of circular dichroism in a pump-probe experiment with a Babinet-Soleil compensator," J. Opt. Soc. Am. B **23**, 2418–2424 (2006).
32. C. Niezborala and F. Hache, "Conformational changes in photoexcited (R)-(+)-1,1′-bi-2-naphthol studied by time-resolved circular dichroism," J. Am. Chem. Soc. **130**, 12783–12786 (2008).